XXVI COLÓQUIO DE USINAGEM

25 a 27 de novembro de 2024, Campinas - SP, Brasil
UNICAMP

TEXTURE BEHAVIOR IN Ni-Cr-Fe ALLOYS BY DIFFERENT LATERAL INFEED MACHINING IN WEDM PROCESS

[1]Giovani Conrado Carlini, giovani.carlini@ifsc.edu.br
[2]Igor dos Santos Roik, igorroik3@unifebe.edu.br
[2]Rodrigo Blödorn, rodrigoblodorn@unifebe.edu.br
[3]Fred Lacerda Amorim, fred.amorim@pucpr.br

[1]Instituto Federal de Santa Catarina - IFSC, Rua dos Imigrantes, 445, Rau 89.254-430, Jaraguá do Sul, SC, Brasil
[2]Centro Universitário de Brusque - UNIFEBE, R. Vendelino Maffezzolli, 333, Santa Terezinha 88352-360, Brusque, SC, Brasil
[3]Pontifícia Universidade Católica do Paraná - PUCPR, Av. Imaculada Conceição, 1155, Prado Velho 80.215-901, Curitiba, PR, Brasil

Abstract. *This study takes a unique approach to investigate and explore the texture of the resolidified layer on Ni-Cr-Fe-based materials that form on surfaces manufactured by wire electrical discharge machining (WEDM). The surfaces were machined while keeping the open voltage, current, and other generator parameters constant. Five grids of lateral feed percentage Δ_y were varied, based on the wire diameter d_w (180 µm), acting directly on the change of the front working clearance with variations of Δ_y = 100%, 75%, 50%, 25%, and 10%. The results show that the lateral feed affects the roughness of Sa and Sz, respectively. Inconel 718 presented the smallest variations and the largest amplitude Sz. The stainless steel AISI 304 resulted in smaller distortions, mainly at Δ_y = 10% and 25%. In both materials, the application of Δ_y = 100% resulted in the worst textures due to the decreased washing efficiency in the working gap. These findings have practical implications for the manufacturing of Ni-Cr-Fe-based materials. An Sdr—Smr_2 mapping was performed for the hybrid and functional characterization of the texture behavior, and no correlations were found between the variation of the tested parameters.*

Keywords*: WEDM, Texture, Lateral infeed, Inconel 718, Stainless Steel AISI 304.*

1. INTRODUÇÃO

Recent engineering applications, particularly those requiring the production of functional parts from advanced materials with heightened mechanical and thermal properties and high corrosion resistance, have created a need for high-precision features. These features must adhere to tight tolerances, high accuracy, complex geometries, and micro parts (Naeim *et al.*, 2023). Our study on the texture behavior in Ni-Cr-Fe alloys by different lateral infeed machining in the WEDM process is significant in this context.

Among the non-conventional processes, Wire Electrical Discharge Machining (WEDM) emerges as a crucial solution to the challenges of processing advanced materials, especially in the context of modern engineering applications. It has evolved into one of the most important production technologies, specifically designed to address the complex task of manufacturing very accurate three-dimensional complex components on any electrically conductive material. WEDM's versatility in machining a wide range of materials, from hardened steels to carbides and ceramic materials, including alloys and superalloys, highlights its applicability (Reolon *et al.*, 2019).

Ni-Cr-Fe alloys are developed to enhance physical, chemical, and technological properties, aiming to achieve materials with high resistance to corrosion and tribocorrosion. Among the various alloys available from manufacturers worldwide, Stainless Steel AISI 304 and Inconel 718 were selected for this research. According to Seshaiah *et al.* (2022), the most popular Stainless Steel is AISI 304. It is widely used because it is easy to manufacture into different shapes and has better corrosion resistance than ordinary steel. Food industry, machine components, textile manufacturing and other domestic and industrial items are made from Stainless Steel AISI 304. The matrix has an austenite characteristic that allows weldability and ductility properties in mechanical forming. Furthermore, it has a non-magnetic characteristic.

Inconel 718 alloys belong to the category of difficult-to-cut alloys by conventional machining processes due to their ability to retain essential properties even at high temperatures, which significantly hinders their machinability. The high heat generated during deformation and friction at the tool-chip and tool-workpiece interfaces makes material removal from the surface of this alloy more difficult (Suárez *et al.*, 2019). Additionally, this alloy tends to harden during deformation, further complicating the machining process. Deformation hardening mechanisms, especially at low feed rates and shallow depths of cut, are often related to high cutting forces that increase wear on the cutting tool's edges (Ezugwu *et al.*, 1998). De Oliveira *et al.* (2020) describe Inconel 718 as a Ni-Cr-Fe alloy employed in numerous components of aero-engines, such as blades, discs, and spindles.

According to Klocke and König (2007), the primary input variables that directly influence the technological process performance and workpiece surface integrity are the average discharge current $\bar{i}_e$ (A), discharge voltage $\bar{u}_e$ (V), and discharge duration t_e (µs). As expressed in Eq. (1), the product of these variables results in the discharge energy W_e (J).

$$W_e = \int_0^{t_e} u_e(t).\, i_e(t).\, dt \tag{1}$$

Consequently, understanding the influence of discharge energy conditions allows for an accurate selection of production parameters. Consequently, understanding the influence of discharge energy conditions allows a precise selection of production parameters on process yield. Furthermore, non-electrical parameters have a great influence on the results, *i.e.*, liquid dielectric grid, pulse train method, and kerf control (Carlini *et al.*, 2022). The evaluation of the lateral increment of the wire has a notable decrease in the literature available for comparison, particularly in relation to scenarios such as the removal of the Inconel 718 alloy and AISI 304 Steel. This lateral variation allows for a distribution of the discharge energy W_e in different sizes of areas. Variations in energy discharge W_e methods result in changing the volume of material removed. Therefore, the wire feed rate v_f [mm/min] and texture quantities must change as they are output variables directly dependent on the process.

According to Czifra and Barányi (2020), certain combinations of surface parameters efficiently characterize surfaces, while others are less so. The best-known correlation refers to the relationship between the arithmetic mean of roughness Ra and the maximum roughness height Rz. These two amplitude parameters depend solely on the height coordinates; they are mathematically independent, but they show correlations in practice. Parameter combinations can be specified in the form of a topological map, which represents the surfaces based on the parameters used for their characterization.

State-of-the-art publications seek parameters to define surface texture when the functional parameters Ra/Sa or Rz/Sz are insufficient to describe a specific application. Pagani *et al.* (2017) described elements to characterize free-form surfaces using three-dimensional parameters such as Sa, Sq, Ssk, Sku, Sdq, and Sdr. They aimed to identify combinations of parameters that could characterize surfaces, forming a topological map. Using a classification matrix and the Spearman correlation technique, Qi *et al.* (2015) defined three-dimensional parameters for surface characterization, creating a mapping that highlights key correlations between a wide variety of parameters, including amplitude, functional, hybrid, and spatial. Podulka *et al.* (2023) described a methodology for reducing errors in texture evaluation.

In recent studies by Carlini *et al.* (2024), correlations were analyzed for textures resulting from Inconel 718 using sink EDM with different electrode materials. They evaluated the peak parameter used for the material component Smr_2 (functional parameter), defined by the distribution of the contact surface under load in relation to the root mean square gradient Sdr (hybrid parameter). Among other results, they concluded that an innovative finding emerged: the Smr_2-Sdr correlation was $\rho = -0.91$, revealing a very strong negative correlation. On surfaces processed by EDM in Inconel 718, smaller distortions lead to higher peak material components. These components correlate to determine the fraction of the surface that can bear the load [%]. The algebraic formula for calculating the functional parameter Smr_2 is presented in Eq. (2),

$$Smr_2 = \frac{A_v}{A_t}\, x\, 100 \tag{2}$$

where A_v is the area of the valleys below a specified height. A_t is the total area of the measured surface. This ratio is then expressed as a percentage to indicate the proportion of the surface area that consists of valleys, while the hybrid parameter Sdr is detailed in Eq. (3),

$$Sdr = \frac{1}{A}\left[\iint_0^A \left(\sqrt{\left[1 + \left(\frac{\partial z(x,y)}{\partial x}\right)^2 + \left(\frac{\partial z(x,y)}{\partial y}\right)^2\right]} - 1\right) dxdy\right] \tag{3}$$

where A = sampling area, $\partial z(x, y)/\partial x$ represents the gradient associated with the point located at x, y along the x-axis, while $\partial z(x, y)/\partial y$ is related to the point located along the y-axis.

In addition to the theoretical description of three-dimensional parameters, Buk (2022) conducted experiments on the removal of Inconel 718 by WEDM, separating it into roughing and finishing operations. The thinning regime involved the complete cutting of a channel with a distribution of 100% of the wire diameter (d_w). For the finishing regime, the lateral infeed (Δ_y) was 30, 50, and 70 µm from wire d_w = 250 µm. It was concluded that lower values did not completely remove the resolidified layer from the previously conducted thinning regime. The smaller Δ_y reduced the roughness without the presence of damage, such as microcracks in the resolidified layer.

The present study investigates the texture resulting from five levels of lateral infeed variations when processing Ni-Cr-Fe alloys using Wire Electrical Discharge Machining (WEDM) while maintaining a consistent discharge energy density. The primary objective is to understand the quantitative results of the surface texture and analyze the influences of electrical removal parameters and variable rates in the discharge area during the manufacture of Inconel 718 and Stainless Steel AISI 304. This aims to elucidate the behavior of three-dimensional amplitude parameters commonly employed in experimental research, such as arithmetical mean height (Sa) and maximum height (Sz). Furthermore, the study evaluates and correlates the functional parameter Smr_2 and the hybrid parameter Sdr to characterize how variations in material properties behave during WEDM removal.

2. EXPERIMENTAL MATERIALS AND METHODS

This study presents a methodology specifically observing the texture resulting from the Wire Electrical Discharge Machining (WEDM) process on two Ni-Cr-Fe alloys when five variations of lateral infeed Δ_y are used. The alloys selected for testing are frequently found in current publications due to their properties and applications in various sectors, including Inconel 718 and Stainless Steel AISI 304. In WEDM operations, the grinding process generally uses a distribution region of 180° in relation to the action of the tool wire, utilizing the nominal d_w diameter. For regrinding or semi-finishing (trim cut) operations, lateral infeed Δ_y is used to reduce manufacturing time compared to finishing time, with reduced discharge energy W_e and smaller roughness amplitude values. From this, the five variables associated with Δ_y were stipulated, keeping the electrical quantities constant, and the topographic changes of the removed surfaces were evaluated. Figure 1 shows the main WEDM definitions found in the VDI standard 3402 (1990).

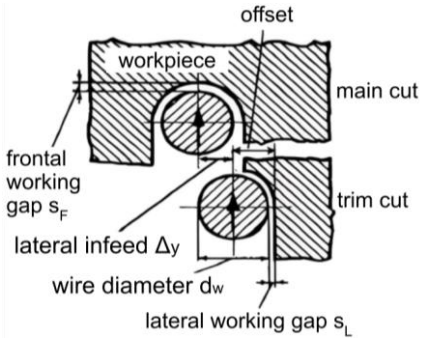

Figure 1. Lateral infeed (Δ_y) and other WEDM definitions from VDI standard 3402 (1990).

2.1. Materials

The machining experiments of WEDM using molybdenum wire on Inconel 718 and AISI 304 were carried out with an isoenergetic generator, maintaining equal independent input variables. These variables included a discharge current $\hat{i}_e$ of 7 A and the open-circuit voltage $\hat{u}_i$ of −70 V (cathode polarity wire). The tests were designed to adequately assess the independent electrical input parameters' effects on technological performance in dielectrics deionized water. The tests were conducted on a GF AgieCharmilles® FW1U CNC 5-axis machine with a wire reuse system using a reciprocating coil. The generator was programmed for isoenergetic pulses. They control the discharge duration t_e and the interval time between pulses t_o. Thus, all discharge control parameters were kept the same in the experiment. Table 1 shows the variables used in the WEDM machine.

Table 1. Independent input variables for the WEDM process.

Variable	Symbol	Value	Unit.
Lateral infeed	Δ_y	10; 25; 50; 75 and 100	%
Discharge voltage	$\hat{u}_i$	-70.0	V
Discharge current	$\hat{i}_e$	7.0	A
Discharge duration	t_e	30.0	µs
Interval time	t_o	75.0	µs
Dielectric inlet pressure	P_{in}	0,25	MPa
Wire tension	-	1200	N/mm^2
Wire diameter	d_w	0.18	mm
Wire run-off speed	W_s	8.0	m/s

The wire feed rate v_f [mm/min] is one of the process output variables and, in relation to the part removal thickness [mm], is used to evaluate the removal efficiency in WEDM. As the thickness increases, the distribution area of the electrical pulses expands, making it more challenging to maintain the cleanliness of the working gap due to contamination from removal byproducts. Consequently, the likelihood of anomalous discharges and a decrease in yield increases with greater thickness and the discharge energy $W_e \approx \hat{u}_e.\hat{i}_e.t_e$ [J] at the same level reduces process performance. Although there are no tribological mechanisms in the process, the chemical, mechanical, and physical properties of each material influence the productivity of the process.

Table 2 presents the chemical composition of the Inconel 718 alloy and Stainless Steel AISI 304 samples. Samples with 10 mm × 10 mm × 50 mm dimensions were machined with a 120 mm cutting perimeter. For each proposed

machining condition, two replicates were performed. The time control for each operation was done through the machine interface.

Table 2. The chemical composition of Alloys. Adapted from Baldin *et al.* (2020) and Naeim *et al.* (2023).

Element [%]	Ni-Cr-Fe Alloys	
	Inconel 718	Stainless Steel AISI 304
Ni	53.0	8.0
Cr	18.0	20.0
Fe	21.0	67.0
C	0.08	0.08
Mn	0.35	2.00
Nb	4.8	-
Al	0.30	-
Mn	0.80	-

As Table 2 shows, the different chemical distributions of the material result from changes in the material properties. Table 3 shows the following mechanical and physical properties that characterize the Ni-Cr-Fe alloys selected for the experiments.

Table 3. Mechanical and physical properties of Ni-Cr-Fe alloys. Adapted from Carlini *et al.* (2022) and Naeim *et al.* (2023).

Properties	Ni-Cr-Fe Alloys		Unit.
	Inconel 718	Stainless Steel AISI 304	
Density	8.2	7.9	g/cm³
Electrical resistivity	125	70	μΩ.cm
Thermal conductivity	11.2	16.2	W/m.K
Thermal expansion	12.1	17.2	$x10^{-6}$/K
Modulus of Elasticity	200	193	GPa
Tensile strength	1426	505	MPa
Melting point	1345	1450	ºC

To achieve effective material removal in the WEDM process, a combination of electrical and non-electrical parameters is essential. According to Thiagarajan (2020) highlights the significant impact of electrical parameters on process performance. While it is common to represent a specific WEDM regime in terms of the discharge energy delivered to the working gap, it is crucial not to overlook the influence of material properties on the process.

2.2. Methods

The machining duration and the wire feed rate v_f [mm/min] for each operation were controlled using the software and interface available on the equipment WEDM. Five grades were conducted, varying the percentage of lateral infeed Δy, based on the diameter of the wire d_w (0.18 mm) and acting directly on changing the frontal working slit with variations of Δy = 100%, 75%, 50%, 25% and 10%. Thus, the width of the electrical discharges through the wire in relation to its diameter resulted in Δy = 180 μm, 135 μm, 90 μm, 45 μm and 18 μm, respectively. Figure 2 schematically represents the arrangement of the lateral infeed Δ_y in the front view (above) and the top view (below).

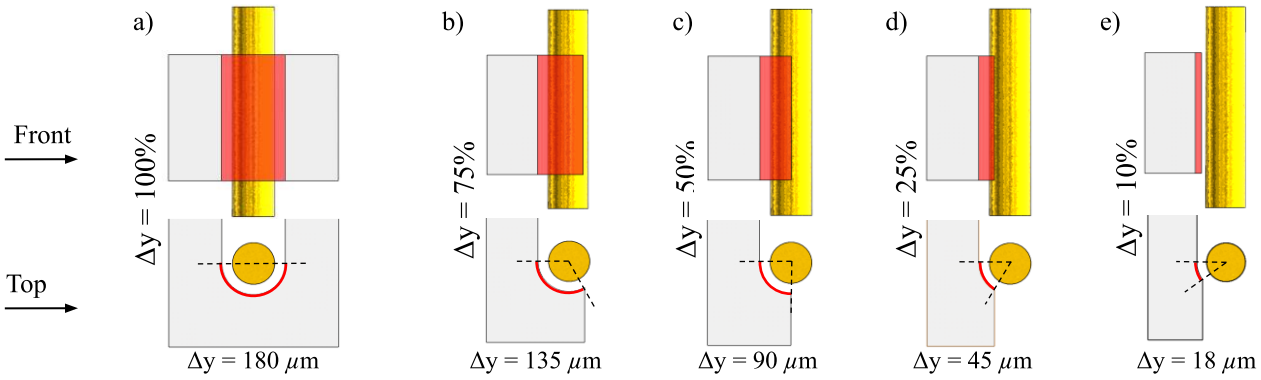

Figure 2. Area of application of electrical discharges when changing the lateral infeed increment (Δ_y).

After the machining process, the samples underwent a thorough cleansing procedure. Initially, they were manually brushed (polyester bristle) and washed, sinking with acetone (C_3H_6O) to eliminate surface byproducts. Subsequently, the samples were subjected to ultrasonic cleaning at a frequency of 40 kHz for 3 min in anhydrous isopropyl alcohol (C_3H_8O). Chemical components were strategically employed to minimize impurities that could affect the precision of subsequent topography and texture measurements.

The analysis of surface texture commences with a detailed examination of the three-dimensional surface morphology using focus variation microscopy (Bruker Alicona® G5) at an optical lens with a 20× magnification, covering an area of 5.0 mm × 5.0 mm. The data is evaluated using the Gaussian filter of the standard ISO 16610-71 order 1 (ISO, 2014). A vertical resolution of 50 nm and a lateral one of 1.5 µm were selected. A 250 µm best-suited cut-off sampling length (λc) with a 1.25 mm profile length was established according to ISO 25178-2 (ISO, 2021). This process generates geometrical surface maps and profile analysis parameters, those investigated in this manuscript: amplitude, functional, and hybrid.

The Alicona MeasureSuite 5.3.1® software was selected to process parameter data. The use of this software ensures accurate and comprehensive analysis of the surface texture and relevant volumetric measurements. The amplitude parameters analyzed were Sa and Sz. Specifically, Sa represents the arithmetic mean of the absolute ordinate Z(x, y) within the selected evaluation area. Furthermore, the maximum height Sz is characterized as the sum of the maximum peak height Sp and the maximum valley depth Sv (Deltombe *et al.*, 2014). According to Czifra and Bárányi (2020), for the functional parameter components, the Firestone-Abbott curve served as the foundational basis, allowing for the collection of relevant data on the rolling area, denoted as Smr_2 (%), as well as the surface distortion percentage, represented by Sdr.

Following the collection of texture measurements, the necessary statistical calculations were performed to determine the Pearson correlation coefficient (ρ). Correlational analysis assesses the relationship between two linear variables, with values ranging from +1 to -1. The sign indicates the direction of the correlation (positive or negative), while the magnitude of the coefficient reflects the strength of the relationship (Guo *et al.*, 2024).

3. RESULTS AND DISCUSSION

The results of this research have practical implications for understanding the behavior of textures in relation to the lateral infeed under the same discharge energy conditions. The working gap, as revealed by this study, causes several effects, particularly regarding the presence of dielectric debris and byproducts in the working gap removed by WEDM. These findings can be applied to mitigate the harmful actions on the integrity of the component after the electrical discharge process, particularly in the field of material science and manufacturing.

Figure 3 shows the textures resulting from the WEDM process in the five lateral advances proposed for removing Inconel 718.

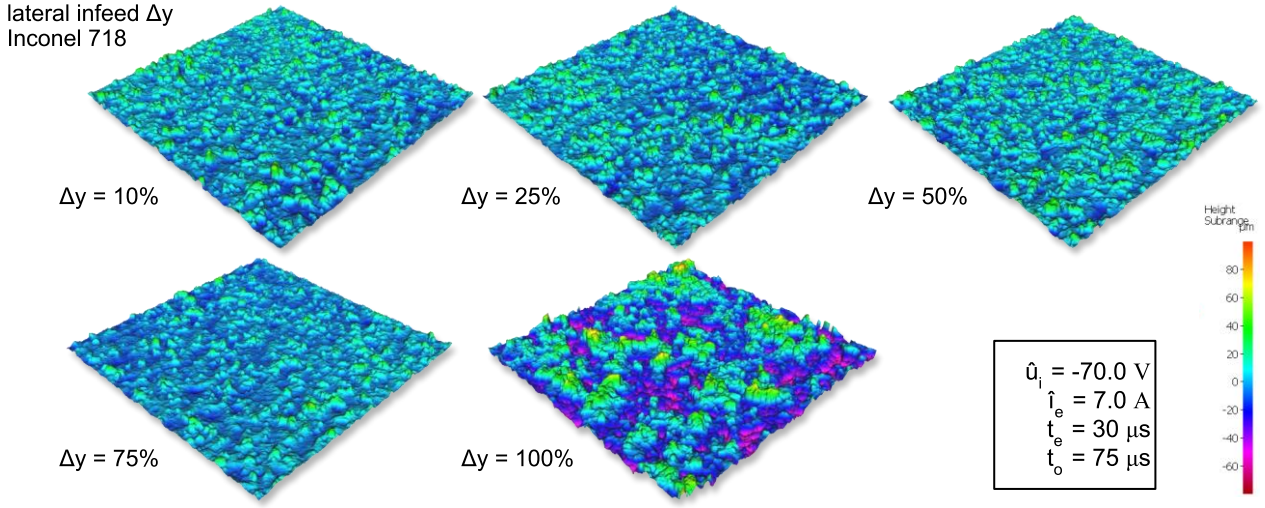

Figure 3. Texture in the area of application of electrical discharges in Inconel 718 when changing the lateral infeed increment Δy = 10% to Δy = 100%.

To perform the topographic characterization of the Inconel 718 texture with WED machining, the selected discharge energy was We = 14.7 mJ. The topographic quantification is obtained by multifocal scanning in the region of interest according to the defined area (5.0 × 5.0 mm). It can be observed that the textures Δy = 10% to 50% do not allow visually

distinguishing the differences, while Δy = 75% presents larger crater regions. Finally, the condition of Δy = 100% shows that the texture has greater distortions.

In turn, Figure 4 shows the textures resulting from the WEDM process in the five lateral advances proposed in the removal of Stainless Steel AISI 304. As the lateral advance increases, the morphology of the resulting textures varies, appearing similar to that observed in Inconel 718.

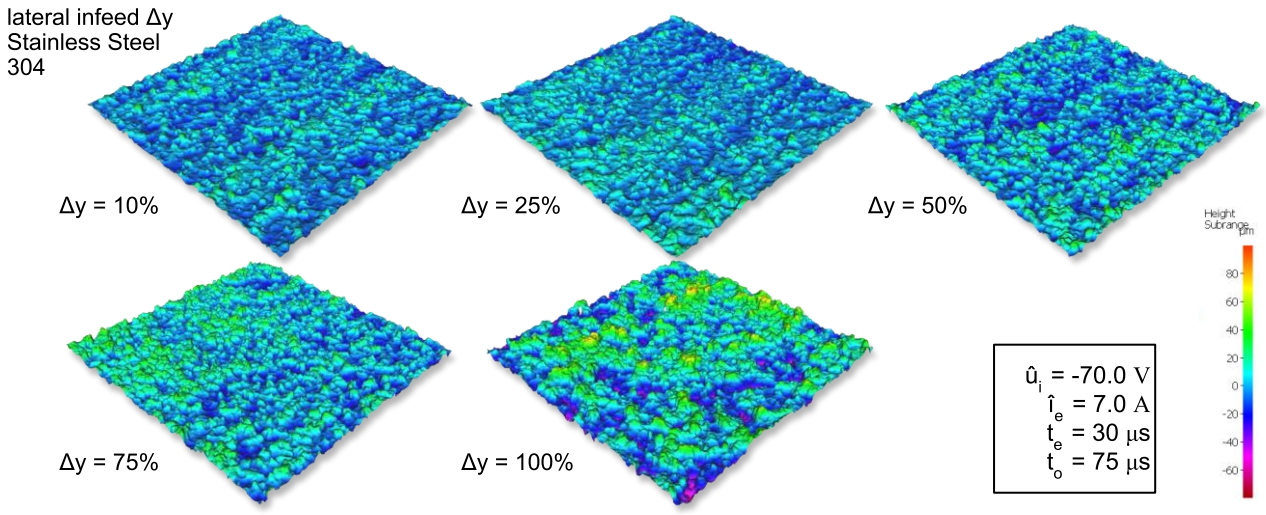

Figure 4. Texture in the area of application of electrical discharges in Stainless Steel AISI 304 when changing the lateral infeed increment Δy = 10% to Δy = 100%.

The surface texture in WEDM results from various combinations of variable parameter conditions. To better characterize the topography of the Inconel 718 and Stainless Steel AISI 304 workpieces, 3D surface roughness parameters, specifically Sa and Sz, representing the arithmetical mean deviation of the assessed profile, are measured (Carlini *et al.*, 2022). These parameters are widely used in industry for in-depth investigations of component texture tolerances and functional performance.

Like what was found in the topographic characterization of the texture of Inconel 718 in the WEDM removal of Stainless Steel AISI 304. The topographic quantification uses the same settings with the defined area (5.0 × 5.0 mm). It can be observed that the textures Δy = 10% to 50% do not allow visually distinguishing the differences, and the condition of Δy = 100% shows that the texture suffered greater distortions. To understand in numerical terms how the texture behaves, amplitude parameters Sa and Sz, as shown in Figure 5.

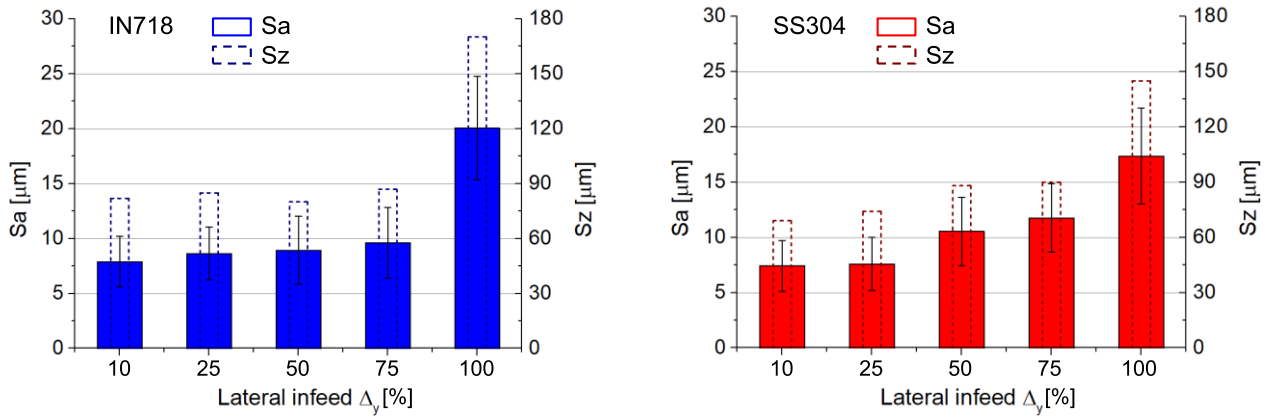

Figure 5. Sa and Sz amplitude parameters with lateral infeed Δy = 10% to Δy = 100%. On the left is the behavior of Inconel 718 (IN718), and on the right is the behavior of Stainless Steel AISI 304 (SS304).

The larger amplitudes shown in Figure 5 present textures that return to the process of greater removal of the component material due to the high discharge energy (roughing). However, it is important to know the variations even in the condition of greater discharge energy to see the size of the damage caused by the thermal removal mechanism (Klocke *et al.*, 2016). Thus, it is possible to know what the excess material should be in the dimensioning for the correct quantification in the subsequent semi-finishing and finishing process.

To better understand this texture behavior, the amplitude parameter Sa (µm) was quantified in addition to the Sz (µm) parameter. In Fig. 5, the roughness measurements Sa show a lower level for Δy = 10% to 100%. This phenomenon occurred in both materials tested. This was possibly due to the physical properties of the sparks and the respective thermal effects on their distribution. In addition, the amount of non-uniform debris in the work flushing during WEDM machining changes as the lateral infeed rises. Thus, higher values of Sa and Sz became larger as a percentage of the wire was in action.

Kunieda and Kitamura (2018) observed the distribution of discharge sites using a transparent electrode made of a single crystal of SiC. They found that the discharge sites were more widely dispersed in water when compared to hydrocarbon dielectric fluid. Additionally, they found that the radial flow of the dielectric fluid due to the discharge can propagate to greater distances from the discharge point, and the oscillation of the bubbles can continue for a longer time in water than in hydrocarbons. Thus, the study sheds light on the ignition and propagation criteria of the electrical discharge in each cycle period. However, it does not address the effects on the topography and integrity of the surface.

In studies on WEDM in Inconel 718, Carlini *et al.* (2022) verified that the increase in the amplitude of the average surface roughness (Sa) presented greater deviations when the discharge energy was increased in both dielectrics tested. However, the lower viscosity of the deionized water resulted in better efficiency in washing the byproducts in the working gap. However, the lateral infeed was not addressed. Thus, lateral infeed studies show that the variation Δy = 10% up to 75% causes little difference in roughness Sa in IN718, while for AISI 304, the variation was slightly greater but still within the error range field.

The amplitude parameter Sz followed the trend of Sa; the highest values were concentrated at Δy = 100%. Inconel 718 exhibited a higher Sz, approaching the wire diameter itself. This observation highlights the challenge of machining materials with high Ni-Cr content, which is less pronounced in AISI 304. The thermal conductivity properties of Inconel 718 are lower, and the efficiency of the electric discharge ends up being restricted. On the other hand, after the fusion is formed, the resolidification process becomes slower, and the formation of peaks and valleys is more pronounced.

Knowing the amplitude deviations on the surface and seeking a better understanding of the topography, the hybrid configurations Sdr and Smr_2 are presented in Fig. 6 and correlated. These clauses are correlated to provide additional information about the resulting topography. By quantifying the Sdr parameter in percentage terms, it is possible to obtain a measure of the increase in surface area. This measure is calculated by comparing the real surface area with the projected area of an ideal flat surface. Therefore, the higher the percentage value, the greater the surface loss becomes. The Sdr values reflect the average magnitude of the surface irregularity gradient and increase as the surface roughness intensifies (Pagani *et al.*, 2017).

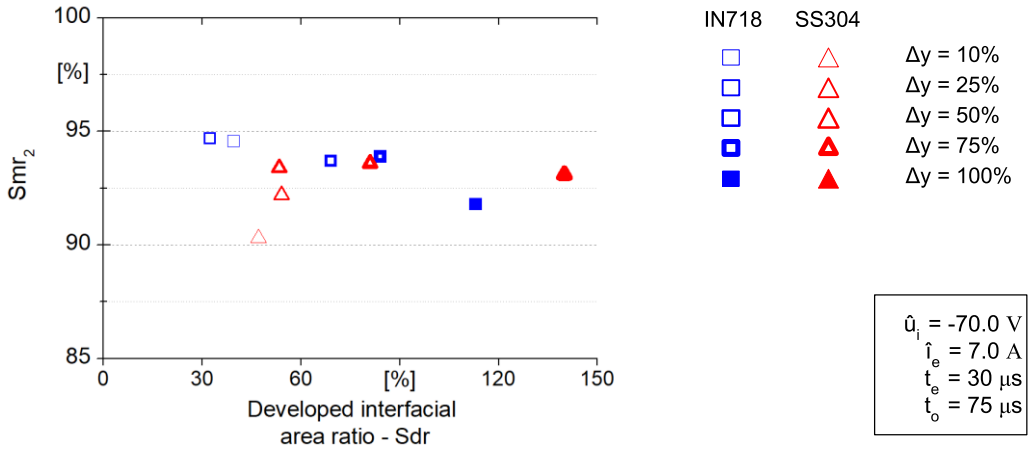

Figure 6. Distribution parameters of Sdr and Smr_2 with lateral infeed Δy = 10% to Δy = 100%.

Analyzing the behavior of Sdr and Smr_2 shown in Figure 6, it can be observed that despite the Sdr values of up to 115% for Inconel 718 and 145% for Stainless Steel AISI 304, the Areal material ratio segmenting protruding valleys from the core Smr_2 are concentrated between 90% and 95%. The variations show that the change does not influence the load-bearing region of the core in the amplitude parameters.

Lateral infeed values lower than 50% showed lower Sdr distortions. However, the variations in Smr_2 were dispersed. To compose the effect together with the two parameters, the Pearson correlation coefficient ρ = -0.18 was calculated, representing a weak negative correlation. Thus, the correlation index for values with large Sdr is not possible to infer or determine the correlation between the parameters. Recent studies have demonstrated that the correlation at lower discharge energy levels can lead to ρ = -0.91. However, in Sdr distortions of up to 15% (Carlini *et al.*, 2024).

When studying the difference in WEDM gap phenomena, the cooling efficiency of the water dielectric is significantly higher. Observation of the distribution of discharge sites shows that discharge sites are more likely to concentrate more efficiently with smaller lateral infeed. This phenomenon explains the behavior for a smaller average surface area Sa (µm).

When machining is stable, the distribution of sparks is efficient, resulting in less roughness distortions (Kunieda & Kitamura, 2018).

Finally, the effects that describe the mechanisms resulting from material removal by WEDM are not yet fully defined. In their publications, the authors contribute to the understanding of the process by indicating directions for describing EDM phenomena and trends for future work. To characterize textures, new analyses on three-dimensional parameters must be performed, identifying behavior patterns and interactions of discharge energy and the workpiece.

4. CONCLUSIONS

This study examines the texture of Ni-Cr-Fe-based materials formed on surfaces manufactured by wire electrical discharge machining (WEDM). Five different lateral infeed rates were used, varying the lateral infeed percentage Δ_y, based on the wire diameter. These variations directly impacted on the change in the work face clearance, with Δ_y values of 100%, 75%, 50%, 25%, and 10%. The topographic analysis of different lateral infeed on Inconel 718 and Stainless Steel AISI 304 is unprecedented. From the results, the following conclusions can be drawn: (i) the results show that lateral infeed affects the surface roughness Sa and Sz, respectively. Inconel 718 showed smaller variations and the largest Sz amplitude. Stainless Steel AISI 304 resulted in smaller distortions, mainly at Δ_y = 10% and 25%; (ii) the application of Δ_y = 100% resulted in the worst textures due to the worsening of the washing efficiency in the working gap in relation to the byproducts promoting anomalous discharge, in both materials; (iii) the Pearson correlation coefficient ρ = -0.18 was calculated, representing a weak negative correlation. This correlation is not characterized due to the large distortion of Sdr, and the independent variables applied in this experimental research aren't present. By this analysis, operations that use the same discharge energy influence the lateral infeed is reduced, mainly in the conditions of full removal.

5. REFERENCES

Baldin, V., Baldin, C. R. B., Machado, A. R., & Amorim, F. L. (2020). Machining of Inconel 718 with a defined geometry tool or by electrical discharge machining. *Journal of the Brazilian Society of Mechanical Sciences and Engineering*, *42*(5), 1–14. https://doi.org/10.1007/s40430-020-02358-7

Buk, J. (2022). Surface Topography of Inconel 718 Alloy in Finishing WEDM. *Advances in Science and Technology Research Journal*, *16*(1), 47–61. https://doi.org/10.12913/22998624/142962

Carlini, G. C., da Silva, C., Torres, R. D., Soares, P., Weingaertner, W. L., & Amorim, F. L. (2022). WED-machining performance by reciprocating molybdenum wire on Inconel 718 with water or hydrocarbon dielectrics. *The International Journal of Advanced Manufacturing Technology*, *119*(3–4), 1853–1866. https://doi.org/10.1007/s00170-021-08386-4

Carlini, G. C., Roik, I. dos S., Blödorn, R., Torres, R. D., & Amorim, F. L. (2024). Beyond the spark: the impact of tool electrode materials, polarities, and pulse distribution on machined surface texture in the electrical discharge machining of Inconel 718 superalloy. *The International Journal of Advanced Manufacturing Technology*, *133*(5–6), 2951–2965. https://doi.org/10.1007/s00170-024-13971-4

Czifra, Á., & Bárányi, I. (2020). Sdq-Sdr Topological Map of Surface Topographies. *Frontiers in Mechanical Engineering*, *6*(July), 1–9. https://doi.org/10.3389/fmech.2020.00050

De Oliveira, D., De Paiva, R. L., da Silva, R. B., & de Carvalho Castro, P. H. (2020). Assessment of the grindability of Inconel 718 under different coolant delivery techniques. *Journal of the Brazilian Society of Mechanical Sciences and Engineering*, *42*(1). https://doi.org/10.1007/s40430-019-2093-0

Deltombe, R., Kubiak, K. J., & Bigerelle, M. (2014). How to select the most relevant 3D roughness parameters of a surface. *Scanning*, *36*(1), 150–160. https://doi.org/10.1002/sca.21113

Ezugwu, E. O., Wang, Z. M., & Machado, A. R. (1998). The machinability of nickel-based alloys: A review. *Journal of Materials Processing Technology*, *86*(1–3), 1–16. https://doi.org/10.1016/S0924-0136(98)00314-8

Guo, P., Xiong, Z., Dong, Z., Zhang, S., Piano, S., & Liu, M. (2024). Multi-parameterised surface texture characterisation for ultra-precision machined surfaces. *Surface Topography: Metrology and Properties*, 0–23. https://doi.org/10.1088/2051-672X/ad6f30

ISO. (2014). *ISO 16610-71*. Geometrical product specifications (GPS) — Filtration — Part 71: Robust areal filters: Gaussian regression filters.

ISO. (2021). *ISO 25178-2*. Geometrical product specifications (GPS) — Surface texture: Areal — Part 2: Terms, definitions and surface texture parameters.

Johny, A., & Thiagarajan, C. (2020). Investigation of surface integrity and it's optimization on pure titanium using molybdenum wire by reciprocated travelling WEDM - A review. *Materials Today: Proceedings*, *33*(xxxx), 2581–2584. https://doi.org/10.1016/j.matpr.2019.12.251

Klocke, F., Hensgen, L., Klink, A., Ehle, L., & Schwedt, A. (2016). Structure and Composition of the White Layer in the Wire-EDM Process. *Procedia CIRP*, *42*(Isem Xviii), 673–678. https://doi.org/10.1016/j.procir.2016.02.300

Klocke, F., & König, W. (2007). *Fertigungsverfahren 3* (5 (ed.)). Abtragen, Generieren und Lasermaterialbearbeitung. Springer Berlin Heidelberg. https://doi.org/10.1007/978-3-540-48954-2

Kunieda, M., & Kitamura, T. (2018). Observation of Difference of EDM Gap Phenomena in Water and Oil Using Transparent Electrode. *Procedia CIRP*, *68*(April), 342–346. https://doi.org/10.1016/j.procir.2017.12.065

Naeim, N., AbouEleaz, M. A., & Elkaseer, A. (2023). Experimental Investigation of Surface Roughness and Material Removal Rate in Wire EDM of Stainless Steel 304. *Materials*, *16*(3). https://doi.org/10.3390/ma16031022

Pagani, L., Qi, Q., Jiang, X., & Scott, P. J. (2017). Towards a new definition of areal surface texture parameters on freeform surface. *Measurement: Journal of the International Measurement Confederation*, *109*, 281–291. https://doi.org/10.1016/j.measurement.2017.05.028

Podulka, P., Macek, W., Branco, R., & Nejad, R. M. (2023). Reduction in Errors in Roughness Evaluation with an Accurate Definition of the S-L Surface. *Materials*, *16*(5). https://doi.org/10.3390/ma16051865

Qi, Q., Li, T., Scott, P. J., & Jiang, X. (2015). A correlational study of areal surface texture parameters on some typical machined surfaces. *Procedia CIRP*, *27*, 149–154. https://doi.org/10.1016/j.procir.2015.04.058

Reolon, L. W., Laurindo, C. A. H., Torres, R. D., & Amorim, F. L. (2019). WEDM performance and surface integrity of Inconel alloy IN718 with coated and uncoated wires. *International Journal of Advanced Manufacturing Technology*, *100*(5–8), 1981–1991. https://doi.org/10.1007/s00170-018-2828-6

Seshaiah, S., Sampathkumar, D., Mariappan, M., Mohankumar, A., Balachandran, G., Kaliyamoorthy, M., Rajendran, B., & Gopal, R. (2022). Optimization on Material Removal Rate and Surface Roughness of Stainless Steel 304 Wire Cut EDM by Response Surface Methodology. *Advances in Materials Science and Engineering*, *2022*. https://doi.org/10.1155/2022/6022550

Suárez, A., Veiga, F., Polvorosa, R., Artaza, T., Holmberg, J., de Lacalle, L. N. L., & Wretland, A. (2019). Surface integrity and fatigue of non-conventional machined Alloy 718. *Journal of Manufacturing Processes*, *48*(August), 44–50. https://doi.org/10.1016/j.jmapro.2019.09.041

VDI. (1990). *VDI 3402*. Elektroerosive bearbeitung: definitionen und terminologie. Deutsches Institut für Normung. Düsseldorf.

6. RESPONSIBILITY FOR INFORMATION

The authors are solely responsible for the information included in this work.